GDQEM Analysis for Free Vibration of V-shaped Atomic Force Microscope Cantilevers

M. H. Korayem[1*], A. Karimi[1], S. Sadeghzadeh[1,2]

1. Robotic Research Laboratory, Center of Excellence in Experimental Solid Mechanics and Dynamics, School of Mechanical Engineering, Iran University of Science and Technology, I.R.Iran
2. School of New Technologies, Iran University of Science and Technology, Tehran, I.R.Iran

(*) Corresponding author: hkorayem@iust.ac.ir

Abstract:

V-shaped and triangular cantilevers are widely employed in atomic force microscope (AFM) imaging techniques due to their stability. For the design of vibration control systems of AFM cantilevers which utilize patched piezo actuators, obtaining an accurate system model is indispensable prior to acquiring the information related to natural modes. A general differential quadrature element method (GDQEM) analysis based on layer-wise displacement beam theory was performed to obtain the natural frequencies of V-shaped AFM cantilevers with piezoelectric actuators. A finite element analysis was applied to validate the accuracy of numerical results. Finally, a parametric investigation of the sensitivity of natural frequencies with respect to beam geometry was performed. Simulations show that presented approach is considerably accurate and does not need a lot computational costs. Based on the governing equations, general differential quadrature method (GDQM) and GDQM could be applied for uniform and stepped plates, respectively. Thus, presented approach covers the V-shaped and triangular cantilevers perfectly and could be utilized to derive the dynamic response of such systems with a little substitution.

Keywords: V-shaped cantilever, Atomic force microscope (AFM), GDQEM.

1. INTRODUCTION

The study of dynamic and static behaviour of atomic force microscope (AFM) cantilevers has become very important for AFM users in recent years. Vibration control of AFM cantilevers is of great interest, especially nowadays which smart structures play a fundamental role in many areas of engineering. One of the best instruments for smart structure actuating and sensing is the piezoelectric patches. Bonding or embedding segments or layers of these materials in a laminated structure would allow the application of strains by which the deformation of the structure could be controlled and/or damped. These patches can be used as sensors as well as actuators. In order to design and implement a vibration control system, an accurate system model is usually required. Specifically, when the state space method is applied, the information related to natural modes is required to solve the respective equations for dynamic response and various control scheme application.

V-shaped and triangular cantilevers are widely employed in AFM imaging techniques due to their stability [1]. As a simple approach, parallel beam method was firstly, presented by Albrecht to approximate the spring constant of V-shaped cantilevers. Consequent to studies of Albrecht, Butt and Sader introduced other equations for the spring constant calculations [3, 4]. Then, Sader proposed another method to enhance the accuracy of his modeling method which leads to the results

closer to those of finite element methods [5]. Although that works responded many questions about the V-shaped cantilevers, geometrical complexity of these cantilevers has caused most investigations and leads to utilizing numerical analyses specifically finite element method with some developments [6-10].

Turner presented a sensitivity evaluation analysis of the bending and torsional vibrations of V-shaped cantilevers [11]. Chang [12] studied the bending vibrations of a rectangular cantilever as a function of the cantilever angle. Later in his studies, Chang assessed the influence of a damper on rectangular cantilever vibration sensitivity [13].

Several discussions have been introduced as controlling and positioning problem for scanning probe devices, especially the dynamic mode AFM [14]. The necessity of real-time imaging in the nanoworld and the high sensitivity of nanoobjects make simulation-based works highly important. So, several modeling and simulation works have been developed. Nowadays, developing the V-shaped cantilever arrays and applications have been increasingly motivated because of emerged technologies and knowledge. As an example, in [15], for measuring concentrated masses or particles, a novel mass sensor incorporating V-shaped cross section cantilever was proposed by locating the analyte at predefined positions for both improving the mass detecting sensitivity and reducing the measuring deviation. In [16], the resonant frequency of flexural vibration for a V-shaped AFM cantilever has been investigated using the Timoshenko beam theory. It has been mentioned that the resonant frequency is sensitive to the width ratio and by increasing this ratio, the resonant frequency decreases, but critical contact stiffness increases, and finally, the variations of the height and breadth taper ratios and width ratio are affected on the sensitivity to the contact stiffness. Also, evaluation of optimum geometric parameters and optimum cantilever slope is considered as a significant purpose in order to obtain maximum flexural sensitivity by using genetic algorithm optimization method [17]. Adopting the parameters for the design of V-shape micro cantilever according to the sample contact stiffness, maximum flexural sensitivity can be obtained, so

that high contrast images are reachable.

These research works could show the significance level of V-shaped cantilevers in micro and nano field studies. The purpose of this study is to investigate the problem of free vibration behavior of V-shaped AFM cantilevers equipped with surface-bonded piezoelectric elements. At first, the mathematical model of the piezoelectric patch is obtained using the Euler-Bernoulli continuous model of a cantilever beam. Then, the V-shaped AFM beam mathematical model derived from parallel beam approximation and based on Euler-Bernoulli assumptions, is solved using differential quadrature element (DQE) analysis technique. This was achieved through discretizing the beam into four elements and solving the subsequent linear equations of the system. Finally, the model is validated utilizing the ANSYS commercial software.

The main contribution of the present work is solution of V-shaped cantilever with an approximately precise method such that it will guarantee the response, and there is no need to solve nonlinear problems for more precision. This could have a great portion on design and manufacturing the advanced arrays and configurations of V-shaped and also other shaped micro cantilevers.

2. GOVERNING EQUATIONS
2.1. Geometrical configuration

Consider a V-shaped cantilever beam composed of a composite substrate with thickness h in its middle and four identical piezoelectric patches with thickness h_p. The patches are perfectly bonded to its upper and lower surfaces as illustrated in Figure 1. Based on the especial applications, the configurations maybe varied but the analysis procedure will be same.

The beam is divided into two parts. The first part from $0 \leq x < \sum_{i=0}^{1} L_i$ with uniform cross section and the second part from $\sum_{i=0}^{1} L_i \leq x < \sum_{i=0}^{3} L_i$ with varying cross section.

The tip is assumed to be located at $x = \sum_{i=0}^{2} L_i$ near the end of the cantilever. The PZT patches are located at the root of cantilever from $0 \leq x < L_0$.
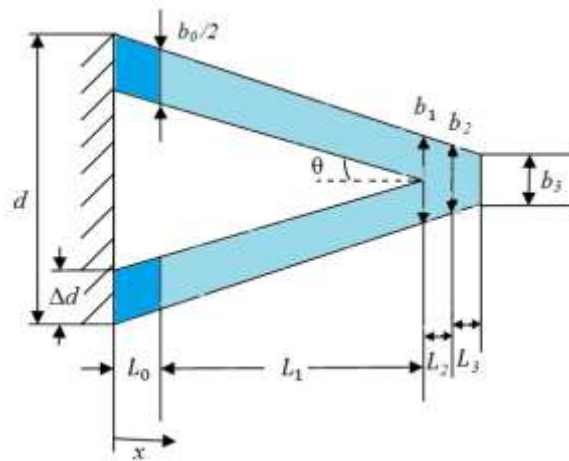
2.2. Equations of motion

The governing equations of the beam in bending vibration and the relevant boundary conditions vary in different regions. For more simplification, four regions are used to define the governing equations and respective boundary conditions. Domain decomposition is the fundamental approach for this system. Because the beam deflection is the most important deformation of V-shaped AFM cantilevers and due to the geometrical complexity, we used the parallel beam approximation (PBA) to derive the equations of motion. In this method, the skewed parts of the beam are considered as parallel Euler-Bernoulli beams. To modify the model, the effective length of beam in skewed sections is considered as follows:
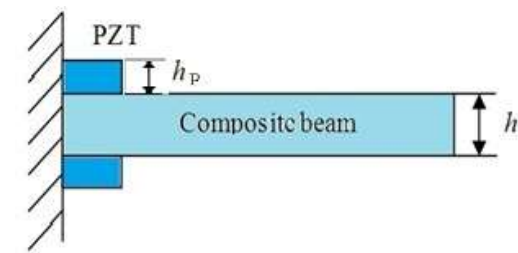
$$L_e = L / Cos\, \theta \qquad (1)$$

where θ is the angle of the beam (Figure 1).

It is assumed that the beam is made of *n* orthotropic laminas which are perfectly bonded together. The beam is relatively thin and the Euler-Bernoulli beam assumptions are acceptable. Based on the Euler-Bernoulli thin beam assumptions, lateral strains are zero ($S_2=S_3=S_4=S_5=0$). Thus, the displacement field can be written as

$$U(x,z) = u(x) - z\frac{\partial w}{\partial x}$$

$$W(x,z) = w(x) \qquad (2)$$

The strains can be written as summation of membrane and bending strains [18].

$$\varepsilon_x = \frac{\partial U}{\partial x} = \frac{\partial u}{\partial x} - z\frac{\partial^2 w}{\partial x^2} = \varepsilon_0 + z\kappa \qquad (3)$$

The linear constitutive relations for the piezoelectric Euler-Bernoulli beam could be given by [18]:

$$\sigma = Q\varepsilon - e^T E$$

$$D = e\varepsilon + \epsilon E \qquad (4)$$

For an *n*-layer one-dimensional beam, equation (2.2.4) could be written as:

$$\sigma_x = \bar{Q}_{11}\varepsilon_x - \bar{e}_{31}E_3 \qquad (5a)$$

$$D_3 = \bar{e}_{31}\varepsilon_x + \bar{\epsilon}_{33}E_3 \qquad (5b)$$

In these equations, σ and D represent the stress and electric displacement; ε and E represent strain and electric field; Q and $\mathcal{E}$ represent the elastic and dielectric permeability coefficients and e is the piezoelectric material coefficient.

The governing equation for the lateral vibration of one-dimensional classic beam is expressed as:

$$\frac{\partial^2 M(x)}{\partial x^2} = \rho A\frac{\partial^2 w}{\partial t^2} \qquad (6)$$

where the moment can be written as:

$$M_{11} = \int_h \sigma_x z\, dz \qquad (7)$$

(a)   (b)

Figure 1. Schematic view of a PZT patch integrated V-shaped beam; (a) Top view, (b) Side view

By using equation (2.2.5a) for an *n*-layer composite beam, we can obtain:

$$M_{11} = \sum_{k=1}^{n} \int \bar{Q}_{11_k} \varepsilon_x z dz - \sum_{k=1}^{n} \int \bar{e}_{31_k} E_{3_k} z dz = M_{11}{}^m + M_{11}{}^e \tag{8}$$

Substituting equation (2.2.3) in to the above relation, yields:

$$M_{11}{}^m = [B_{11}{}^m, D_{11}{}^m] \cdot \begin{bmatrix} \varepsilon_0 \\ \kappa \end{bmatrix} \tag{9}$$

Due to dimensional symmetry, $B_{11}{}^m = 0$ and hence:

$$D_{11}{}^m = \frac{1}{3} \sum_{k=1}^{n} \bar{Q}_{11_k} (z_k^3 - z_{k-1}^3) \tag{10}$$

By applying the Hamilton's principle, it can be found that:

$$\frac{\partial D_{3_k}}{\partial z} = 0 \Rightarrow D_{3_k} = Q^*{}_{3_k} \tag{11}$$

where $Q^*{}_{3k}$ is the electrostatic charge on the surfaces of piezoelectric layers. It should be noted that the in-plane electric fields E_1 and E_2 are assumed zero in the thin piezoelastic laminated beam. It can be expressed as [18]:

$$D_{3_k} = \bar{e}_{31_k} \varepsilon_x + \bar{\epsilon}_{33_k} E_{3_k} \tag{12}$$

Thus

$$E_{3_k} = \frac{D_{3_k}}{\bar{\epsilon}_{33_k}} - \frac{1}{\bar{\epsilon}_{33_k}} * (\bar{e}_{31_k} \varepsilon_x) \tag{13}$$

With the assumption of zero electrostatic charge on the piezoelectric layers, the following is obtained:

$$E_{3_k} = -\frac{1}{\bar{\epsilon}_{33_k}} * (\bar{e}_{31_k} \varepsilon_x) \tag{14}$$

Using equations (8) and (14), and integrating gives:

$$M_{11}{}^e = \sum_{k=1}^{n} \int \bar{e}_{31_k} E_{3_k} z dz$$

$$D_{11}{}^e = \frac{1}{3} \sum_{k=1}^{n} \left(\frac{-\bar{e}_{31}^2}{\bar{\epsilon}_{33}}\right)_k (z_k^3 - z_{k-1}^3) \tag{15}$$

The moment in each cross section of the beam is expressed as:

$$M(x) = b(x) \cdot M_{11} = b(x) \cdot (M_{11}{}^m + M_{11}{}^e) \tag{16}$$

in which *b* represents the width of the cross sections. Combining equation (2.2.6) and equation (2.2.16) gives the equation of motion for the kth piezoelastic layer:

$$(D_{11}{}^m + D_{11}{}^e)_k \frac{\partial^2}{\partial x^2} \left[b_k(x) \frac{\partial^2 w}{\partial x^2}\right] + \rho_k A_k(x) \frac{\partial^2 w}{\partial t^2} = 0 \tag{17}$$

Now, we consider the beam geometry and divide the beam into four elements. The beam equation of motion can be derived by applying equation (2.2.17) on each element and integrating those equations with respect to the thickness.

For the first element with constant cross section we have:

$$(D_{11}{}^m + D_{11}{}^e)_1 \frac{\partial^4 w_1}{\partial x^4} + I_1 \frac{\partial^2 w_1}{\partial t^2} = 0 \qquad 0 \le x < L_0 \tag{18}$$

And the mass-related term is defined as:

$$I_1 = \sum_{k=1}^{n} \int_{z_{k-1}}^{z_k} \rho^{(k)} dz \tag{19}$$

Boundary conditions could be obtained by geometrical characteristics of the beam.

$$w_1(0,t) = 0, \qquad \left.\frac{\partial w_1}{\partial x}\right|_{x=0} = 0 \tag{20}$$

Subsequently for the second element it can be written:

$$(D_{11}{}^m)_2 \frac{\partial^4 w_2}{\partial x^4} + I_2 \frac{\partial^2 w_2}{\partial t^2} = 0 \qquad L_0 \le x < \sum_{i=0}^{1} L_i \tag{21}$$

The boundary and compatibility equations are defined as:

$$w_1(L_0^-, t) = w_2(L_0^+, t)$$

$$\frac{\partial w_1(L_0^-, t)}{\partial x} = \frac{\partial w_2(L_0^+, t)}{\partial x}$$

$$M_x(L_0^-, t) = M_x(L_0^+, t)$$

$$V_x(L_0^-, t) = V_x(L_0^+, t) \tag{22}$$

In the third element, the cross section varies from left to right. According to Figure 2 for an arbitrary cross section, it follows that:

$$b(x) = b_1 \left[1 - \eta_1 \frac{x_2}{L_2}\right]$$

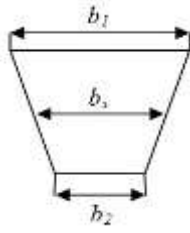$$x_2 = x - (L_0 + L_1)$$

$$\eta_1 = 1 - \frac{b_2}{b_1} \tag{23}$$

Korayem *et al.*

Figure 2. *Geometry of an arbitrary cross section in the third element*

$$(D_{11}{}^m)_3 \frac{\partial^2}{\partial x_2^2}\left[\left(1 - \eta_1 \frac{x_2}{L_2}\right)\frac{\partial^2 w_3}{\partial x_2^2}\right] + I_2\left(1 - \eta_1 \frac{x_2}{L_2}\right)\frac{\partial^2 w_3}{\partial t^2} = 0 \qquad 0 \leq x_2 < L_2 \qquad (24)$$

Boundary and compatibility equations are expressed as:

$$w_2(L_1{}^-,t) = w_3(L_1{}^+,t)$$

$$\frac{\partial w_2(L_1{}^-,t)}{\partial x_2} = \frac{\partial w_3(L_1{}^+,t)}{\partial x_2}$$

$$(D_{11}{}^m)_4 \frac{\partial^2}{\partial x_3^2}\left[\left(1 - \eta_2 \frac{x_3}{L_3}\right)\frac{\partial^2 w_4}{\partial x_3^2}\right] + I_2\left(1 - \eta_2 \frac{x_3}{L_3}\right)\frac{\partial^2 w_4}{\partial t^2} = 0 \qquad 0 \leq x_3 < L_3 \qquad (26)$$

$$w_3(L_2{}^-,t) = w_4(L_2{}^+,t)$$

$$\frac{\partial w_3(L_2{}^-,t)}{\partial x_3} = \frac{\partial w_4(L_2{}^+,t)}{\partial x_3}$$

$$M_x(L_2{}^-,t) = M_x(L_2{}^+,t)$$

$$V_x(L_2{}^-,t) = V_x(L_2{}^+,t)$$

$$M_x(L_3,t) = 0$$

$$V_x(L_3,t) = 0 \qquad (27)$$

where $\eta^2 = 1 - b_3/b_2$.

2.3. GDQEM Analog

The differential quadrature (DQ) method is a discrete approach towards a direct solution of engineering and mathematic governing equations. Since it utilizes higher order polynomials in general coordinates and approximates a function derivative in a given point of its domain directly, it is superior to other FD and FE methods. On the other hand, high level of accuracy and the application convenience of this method have led to its increasing popularity.

By using the DQ technique, the numerical statement of the problem does not pass through any variational formulation, but deals directly with the

Thus, the equation of motion is derived by combining equation (17) and equation (23) as:

$$M_x(L_1{}^-,t) = M_x(L_1{}^+,t)$$

$$V_x(L_1{}^-,t) = V_x(L_1{}^+,t) \qquad (25)$$

And finally for the last element:

governing equations of motion. A major drawback of the conventional DQ method is its difficulty in application to differential equations with multiple boundary conditions at boundary points. General differential quadrature element method (GDQEM) is a more advanced theory that can be used for the beams with discontinuities in geometry and material properties. Referring to the formulation of the equilibrium equations of V-shaped AFM cantilevers, the system of fourth-order partial differential equations are solved. The discretization of the system by means of the GDQEM procedure leads to a linear system of equations, where four independent variables are involved for each element.

By applying the GDQE method to the equation of motion of beam's first region, it follows that:

$$(D_{11}{}^m + D_{11}{}^e)_1 \sum_{j=1}^{n} c_{1_{ij}}^{(4)} W_{1j} + \omega_i^2 I_1 W_{1i} = 0$$

$$(28)$$

And for the boundary conditions:

$$W_{1_1} = 0$$

$$\sum_{j=1}^{n} c_{1_{1,j}}^{(1)} W_{1j} = 0 \qquad (29)$$

Finally by discretizing the beam's equations of motion and boundary equations and solving the resulted linear system of equations it could be

obtained [18]:

$$A_{IB}W_B + A_{II}W_I = -I\omega^2 W_I \qquad (30a)$$

$$A_{BB}W_B + A_{IB}W_I = 0 \qquad (30b)$$

where W_B and W_I are displacement vector of boundary and domain nodes, respectively. Also A_{ij} represent the coefficient vector of W_j for the nth domain equation.

By replacing W_B from equation (30b) into equation (30a), it could be found [18]:

$$\left(A_{II} - A_{IB}A_{BB}^{-1}A_{BI}\right)W_I = -I\omega^2 W_I \qquad (31)$$

The above equation is an eigen value problem. By solving this equation, natural frequencies and mode shapes of the beam could be obtained.

3. NUMERICAL RESULTS AND DISCUSSIONS
3.1. Comparison and verification- rectangular cantilevers

There exist some numerical solutions for electromechanical problems. The finite element method (FEM) is commonly used to study the behavior of MEMs and even NEMs. Previously, validation had been provided by comparison of methods with the traditional softwares such as ANSYS and ABAQUS. Here, for more clarification, comparisons for the static and dynamic responses have made with the Green's function approach and ANSYS software. In ANSYS, the shell element has been used. These comparisons clearly show the efficiency of the proposed model. Table 1 lists the properties and dimensions of beams and plates that have been used for comparison. Table 2 lists the static deflection of the midpoint of beam and plate due to the point and uniformly distributed loads. For each problem, simulation error of GDQM is of considerably lower order compared to the FEM.

3.2. Dynamic responses

Dynamic response of A-beam (middle point) under the SS-SS boundary conditions due to a uniformly distributed load (as $100\times Sin$ $(10\times t)$) has been compared in Figure 2. Figure 3 shows the dynamic response of A-plate (middle point) under SS-SS-SS-SS boundary conditions, due to a uniformly distributed load (as $100\times Sin$ $(10\times t)$). In Figure 2, three approaches resulted in same responses, when in the case of plate (Figure 3), the GDQ method leads to more accurate estimation.

Consequently, according to more accuracy of GDQ, it is used for the dynamic response in nano metric operations. As already discussed, the exact solution cannot be provided in the case of other boundary conditions. On the other hand, however, the GDQ results could be compared with FEM with an intrinsic guarantee in accuracy for both static and dynamic responses. Based on the mentioned comparisons, reliability of the presented approaches is satisfied. So, it can be used to study the various parameter effects on the performance of MEMs and NEMs.
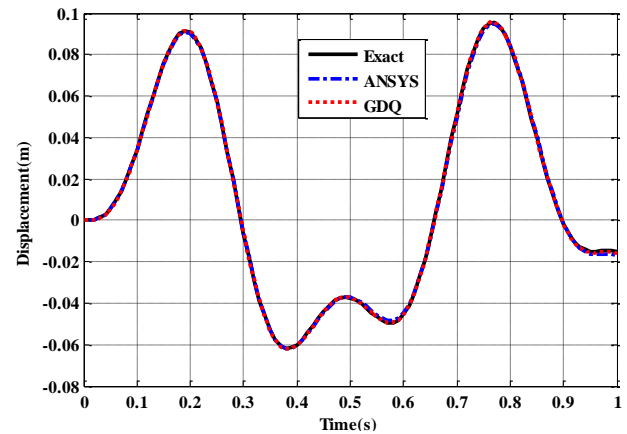

Figure 3. *Dynamic response for beam; comparison of exact, ANSYS and GDQ models*

3.3. Comparison and verification– V-shaped cantilevers

To validate the present DQEM analysis, we consider a graphite-epoxy V-shaped beam with PZT actuators. The first three non-dimensional natural frequencies (NDNF) for given materials and dimensions in Table 1, are presented in Table 2.

Note that:

$$NDNF = \sqrt{\frac{\omega^2 L^4 b_0 \sum \rho_i h_i}{\sum E_i I_{0_i}}}$$

Korayem *et al.*

Table 1. *Properties of beams and plates used for simulations*

Problem	Dimensions (m)	Module of Elasticity (G Pa)	Density (Kg/m³)	Configuration
A-Beam	5×0.04×0.04	70	2800	Simple
B-Beam	2.5×0.04×0.04,2.5×0.04×0.06	70	2800	Step
A-Plate	1×1×0.03	70	2800	Simple
B-Plate	0.5×1×0.03,0.5×1×0.05	70	2800	Step
Problem	Dimensions(m)	Piezo Type	Material	Configuration
C-Plate	0.1×.05×.0025	PZT-5H	Gr/Epoxy	Simple
D-Plate	0.05×0.05×0.0025, 0.05×0.05×0.0015	PZT-5H	Gr/Epoxy	Step

Table 2. *Comparison of present approach, exact and ANSYS results for static problem*

System and BC	Loading	Exact	ANSYS		GDQM	
			δ	Er. (Ans-Exct) (%)	δ (mm)	Er. (DQ-Exct) (%)
A-Beam, SS-SS	Point load on mid	17.43861607	17.386 mm	0.30172	17.43861 mm	0
A-Beam, SS-SS	Distributed Load	54.49567	54.278 mm	0.39943	54.49567 mm	0
A-Plate, SS-SS-SS-SS	Distributed Load	2.34713e-3	2.5654e-3 mm	9.299442	2.35808e-3 mm	0.466
System and BC	**Loading**		**ANSYS**	**GDQEM**	**Er.(Ans-DQ) (%)**	
B-Beam, C-F	Point load on end		0.025835 m	0.025834986	0.0	
B-Beam, C-SS	Point load on mid		0.0040965 m	0.00410869	0.3	
B-Beam, C-C	Point load on mid		0.0025456 m	0.00255845	0.5	
B-Beam, C-F	uniform line load		0.17856 m	0.178019 m	0.3	
B-Beam, C-SS	uniform line load		0.012003 m	0.01200315 m	0.0	
B-Beam, C-C	uniform line load		0.0063912 m	0.006396139 m	0.0	
B-Plate, C-C-C-F	uniform line load		1.0852 µm	1.113778 µm	2.0	
B-Plate, C-C-C-C	uniform line load		0.69290 µm	0.711344 µm	2.0	
B-Plate, C-SS-SS-C	uniform line load		1.0432 µm	1.07712 µm	3.1	

3.4. Study of convergence

To demonstrate the stability, the rate of convergence and accuracy of the results, the first three non-dimensional natural frequencies are illustrated in Figure 3. Because the order of system equations is four, the smallest number of grid points for each element is five. By increasing the number of grid points of elements, it is observed that the results have excellent rate of convergence without instability for an increasing number of grid points. Also by comparing the results with FEM solutions, one can conclude that the solutions have excellent accuracy with a few number of grid points.

3. 5. Effect of the geometrical parameters on the natural frequency

After validating the present model, a parametric investigation was initiated. In order to investigate the effect of length, one non-dimensional parameter Λ was used. By using this parameter, all the results are independent of the beam and piezo patches length. The length parameter is defined as:

$$\Lambda = \frac{\text{Length of piezo patch}}{\text{Length of composite skewed arm}} = \frac{L_0}{L_1}$$

Figure 4 shows the variation of the first three non-dimensional frequencies in comparison with the beam non-dimensional length. The results indicate, as expected, that with increasing the Λ, due to piezoelectric stiffening effect, NDNF has increased. Also it is obvious that the length parameter has considerable effect on the higher natural frequencies.

The second geometrical parameter is beam non-dimensional width Δ, which is defined as the ratio of skewed arm width to the distance between arms at the beam root:
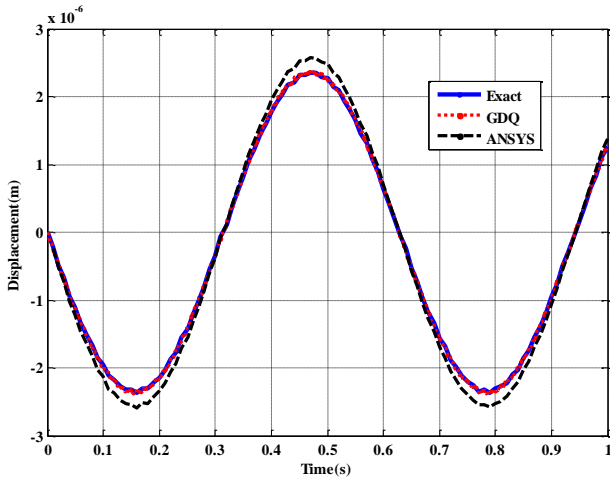
$$\Delta = \frac{\Delta d}{d}$$

Figure 4. *Dynamic response for plate; comparison of exact, ANSYS and GDQM*

It is concluded from Figure 5 that increasing beam width causes an increasing effect on the NDNF. Figure 6 shows variation of NDNF in respect to the non-dimensional thickness H, which is expressed as the actuator thickness to beam thickness.
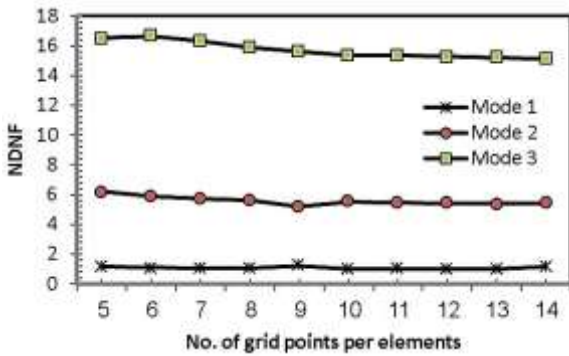
$$H = \frac{h_p}{h}$$

Figure 5. *Variation of first three NDNF in comparison with No. of grid points*

As it is obvious from Figure 6, non-dimensional thickness has a maximum effect on NDNF at H≈ 0.3. Since at the beginning, with increasing the thickness, the overall beam stiffness will raise, but by more increase in thickness, the local actuators' stiffness grow extremely and actuators act as a solid boundary. So the effective length of beam and subsequently NDNF will decrease.
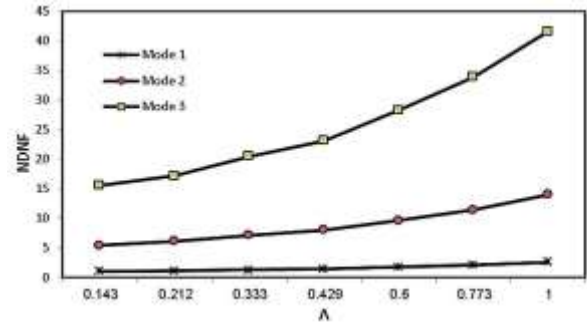

Figure 6. *Effect of beam length on NDNF (θ=30°)*

It is concluded from beam geometry that cantilever angle does not have an independent effect and its variation is directly related to beam length. As it is observed from Table 3, with increasing the beam angle, the effective beam length has increased and subsequently the non-dimensional length and NDNF has decreased.

Table 3. *Material properties used for T300/5208 graphite-epoxy and PZT*

Property	Carbon/epoxy	PZT
E_1 (GPa)	154.0	63.0
E_2 (GPa)	11.13	63.0
v_{12}	0.304	0.3
G_{12} (GPa)	6.98	24.2
G_{13} (GPa)	6.98	24.2
G_{23} (GPa)	3.36	24.2
Ply thickness (mm)	0.3	0.1
ρ (kg/m^3)	1560	7600
e_{31} (N/V mm)	-	0.0229

Figure 7 shows the variation of first three NDNF versus composite layer fibers angle. The results indicate that the NDNF is symmetric with respect to the angle about 90.
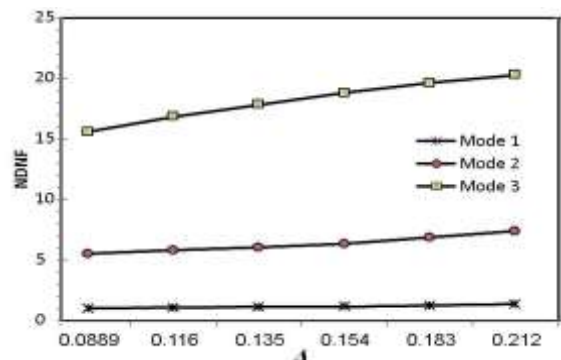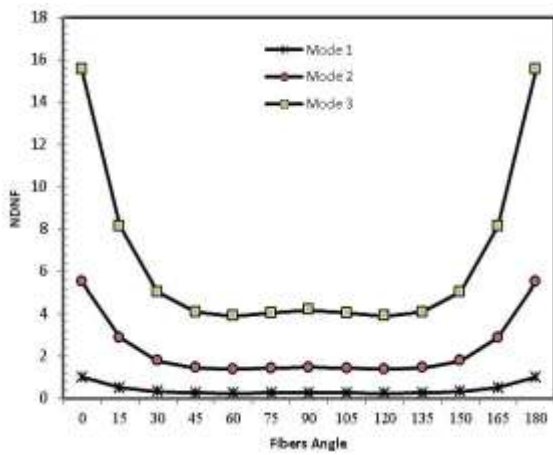

Figure 7. *Effect of beam width on NDNF (θ=30°)*

Korayem *et al.*

Figure 8. *Variation of NDNF vs. Fibers angle (θ=30°)*

Table 4. *Comparison of non-dimensional natural frequencies obtained with present method and ANSYS software*

	DQEM	ANSYS	Difference
1st NDNF	1.0237	1.0528	2.8%
2nd NDNF	5.5314	5. 6199	1. 6%
3rd NDNF	15.730	15.921	1.2%

Table 5. *First three NDNF versus beam angle*

2θ (Degree)	30°	45°	60°	75°	90°
1st NDNF	1.0237	1.0223	1.0202	1.0182	1.0158
2nd NDNF	5.5314	5.5289	5.5244	5.5200	5.5162
3rd NDNF	15.730	15.656	15.561	15.455	15.352

4. CONCLUSIONS

In this study, the bending-free vibration of a V-shaped AFM cantilever which partially bonded with piezo actuators was investigated. We used the GDQE method for simultaneous simplicity and accuracy to analyze the mathematical model derived from parallel beam approximation and based on Euler-Bernoulli assumptions. Convergence and comparison studies were performed to verify the accuracy and merit of the present method. The numerical results show the dependency of fundamental natural frequencies to the geometrical parameters of the beams. Ultimately, it was observed that geometrical parameter may significantly affect the free vibration behavior.

REFERENCES

1. J. E. Sader and J. R. Friend, "Note: Calibration of atomic force microscope cantilevers using only their resonant frequency and quality factor," *Review of Scientific Instruments.,* vol. 85, (2014), pp. 116101-116101-3.

2. T. Albrecht, S. Akamine, T. Carver, and C. Quate, "Microfabrication of cantilever styli for the atomic force microscope," *Journal of Vacuum Science & Technology A.,* vol. 8, (1990), pp. 3386-3396.

3. H. J. Butt, P. Siedle, K. Seifert, K. Fendler, T. Seeger, E. Bamberg, *et al.*, "Scan speed limit in atomic force microscopy," *Journal of microscopy.,* vol. 169, (1993), pp. 75-84.

4. J. E. Sader and L. White, "Theoretical analysis of the static deflection of plates for atomic force microscope applications," *Journal of Applied physics.,* vol. 74, (1993), pp. 1-9.

5. J. E. Sader, "Parallel beam approximation for V-shaped atomic force microscope cantilevers," *Review of Scientific Instruments.,* vol. 66, (1995), pp. 4583-4587.

6. T. Drobek, R. Stark, M. Gräber, and W. Heckl, "Overtone atomic force microscopy studies of decagonal quasicrystal surfaces.," *New Journal of Physics.,* vol. 1, (1999), p. 15.

7. T. Drobek, R. W. Stark, and W. M. Heckl, "Determination of shear stiffness based on thermal noise analysis in atomic force microscopy: passive

overtone microscopy.," *Physical Review B,* vol. 64, (2001), p. 045401.

8. M. Stark, R. W. Stark, W. M. Heckl, and R. Guckenberger, "Spectroscopy of the anharmonic cantilever oscillations in tapping-mode atomic-force microscopy," *Applied Physics Letters.,* vol. 77, (2000), pp. 3293-3295.

9. G. Yaralioglu, F. Degertekin, K. Crozier, and C. Quate, "Contact stiffness of layered materials for ultrasonic atomic force microscopy," *Journal of Applied Physics.,* vol. 87, (2000), pp. 7491-7496.

10. G. Yaralioglu, A. Atalar, S. Manalis, and C. Quate, "Analysis and design of an interdigital cantilever as a displacement sensor," *Journal of Applied Physics.,* vol. 83, (1998), pp. 7405-7415.

11. J. A. Turner and J. S. Wiehn, "Sensitivity of flexural and torsional vibration modes of atomic force microscope cantilevers to surface stiffness variations," *Nanotechnology.,* vol. 12, (2001), p. 322.

12. W.-J. Chang, "Sensitivity of vibration modes of atomic force microscope cantilevers in continuous surface contact," *Nanotechnology.,* vol. 13, (2002), p. 510.

13. W.-J. Chang, T.-H. Fang, and H.-M. Chou, "Effect of interactive damping on sensitivity of vibration modes of rectangular AFM cantilevers," *Physics Letters A.,* vol. 312, (2003), pp. 158-165.

14. M. Korayem, S. Sadeghzadeh, and A. Homayooni, "Coupled dynamics of piezo-tube and microcantilever in scanning probe devices and sensitive samples imaging," *Micro & Nano Letters, IET.,* vol. 7, (2012), pp. 986-990.

15. R. Gao, Y. Zhang, J. Zhao, and S. Liu, "A novel V-shaped cross section cantilever sensor for monitoring concentrated masses with improved detecting sensitivity and measuring accuracy," (2014).

16. A. Sadeghi, "The flexural vibration of V shaped atomic force microscope cantilevers by using the Timoshenko beam theory," *ZAMM-Journal of Applied Mathematics and Mechanics/Zeitschrift für Angewandte Mathematik und Mechanik.,* vol. 92, (2012), pp. 782-800.

17. S. Moeini, M. Kahrobaiyan, M. Rahaeifard, and M. Ahmadian, "Optimization of First Mode Sensitivity of V-Shaped AFM Cantilever Using Genetic Algorithm Method," in *ASME 2009 International Mechanical Engineering Congress and Exposition*, (2009), pp. 495-501.

18. M. Korayem, S. Sadeghzadeh, and A. Homayooni, "Semi-analytical motion analysis of nano-steering devices, segmented piezotube scanners," *International Journal of Mechanical Sciences.,* vol. 53, (2011), pp. 536-548.